Translational and rotational diffusion of model nanocolloidal dispersions studied by molecular dynamics simulations



1998 J. Phys.: Condens. Matter 10 10159

(http://iopscience.iop.org/0953-8984/10/45/005)

J. Phys.: Condens. Matter **10** (1998) 10159–10178. Printed in the UK PII: S0953-8984(98)94600-8

# Translational and rotational diffusion of model nanocolloidal dispersions studied by molecular dynamics simulations

D M Heyes†, M J Nuevo‡, J J Morales‡‖ and A C Brańka§

† Department of Chemistry, School of Physical Sciences, University of Surrey, Guildford GU2 5XH, UK

‡ Departamento de Física, Facultad de Ciencias, Universidad de Extremadura, 06071 Badajoz, Spain

§ Institute of Molecular Physics, Polish Academy of Sciences, Smoluchowskiego 17/19, 60-179 Poznań, Poland

Received 27 May 1998, in final form 15 September 1998

**Abstract.** Molecular dynamics (MD) simulations have been used to study the translational and rotational relaxation of model spherical nanocolloidal particles in solution at infinite dilution. The solvent was modelled at the molecular level. Simulations were carried out with two types of model nanocolloidal particle, one that was smooth ('structureless') and the other built from a cluster of atoms ('rough'). Both types had variable diameter, $\sigma_c$, compared to that of the solvent molecule, $\sigma_s$. The Weeks–Chandler–Andersen (WCA) interaction between the colloid and the WCA solvent molecules was used. Nanocolloidal particles that were up to an order of magnitude larger than those of the solvent molecules were simulated. The effects of the relative solvent and colloidal particle mass density, and colloid size on the translational and rotational self-diffusion coefficients were investigated. At liquid-like number densities ($\rho_s = N\sigma_s^3/V \simeq 0.9$) the translational, $D$, and rotational, $D_{rot}$, self-diffusion coefficients for the nanocolloids of all sizes were statistically independent of the ratio of colloidal to solvent particle mass density for the the values, up to $\simeq$4.0, explored. As solvent number density decreased, the translational self-diffusion coefficients of the colloidal particles showed more evidence than the rotational self-diffusion coefficients of a decrease with increasing colloid particle density. Both $D$ and $D_{rot}$ decreased with increasing size of the colloidal particle in close agreement with the classical solutions, the Stokes–Einstein and Stokes–Einstein–Debye relationships respectively. Differences in the translational diffusion coefficients of smooth and rough colloidal particles were not statistically significant at $\rho_s = 0.9$, but at $\rho_s = 0.7$ the $D$ were lower for the rough particles. Reorientational motion occurred by small-step diffusion.

## 1. Introduction

The complexity of colloidal liquids prohibits exact analytic treatments of their dynamical and physical properties in all but the most idealized of cases (e.g., macroscopic spheres at infinite dilution). There are now a number of so-called *mesoscale* discrete particle simulation techniques that have been developed to provide approximate treatments of these systems, which treat the faster solvent degrees of freedom in an approximate way, concentrating on the slower (usually more important) degrees of freedom associated with the colloidal particle's translational and, sometimes, rotational trajectories. Examples of such techniques

‖ Deceased.

0953-8984/98/4510159+20$19.50  

include Brownian dynamics (Ermak 1975), and lattice Boltzmann (Benzi *et al* 1992) and dissipative particle dynamics (DPD) (Marsh *et al* 1997). A problem with these techniques at finite colloid volume fraction is that, because of the slow decay of hydrodynamic effects (with an $\sim r^{-1}$ distance dependence), the consequences of truncation effects in approximate treatments are rather difficult to quantify and consequently there is no near-exact solution for the dynamics of dense suspensions.

With recent advances in computer power it has now become feasible to study the dynamical behaviour and other physical properties of nanocolloid liquids using the molecular dynamics, MD, method (Hansen and McDonald 1986). (Nanocolloid liquids contain small colloidal particles in the nm range.) MD can be used to simulate both the colloidal particles and solvent molecules simultaneously by numerical integration of Newton's equations of motion for all molecules in the system. It therefore has fewer assumptions than the mesoscale modelling methods, and can give much more detail (for example, it automatically incorporates the many-body hydrodynamic effects), but of course currently is limited to much smaller model colloidal particles. With present-day computational resources, MD is limited to exploring the transition region between simple liquids and typical colloidal liquids (i.e., where the particles are in the 0.1–1 $\mu$m range) which is nevertheless an interesting region because it encompasses the regime in which several characteristic timescales, which can be well separated for micron-sized colloidal particle systems, overlap.

The Stokes–Einstein and Stokes–Einstein–Debye formulae provide a good theoretical description for, respectively, translational and rotational diffusion of micron-sized spheres in the infinite-dilution limit (Hansen and McDonald 1986). No satisfactory comparable treatment for nanocolloidal particles exists, and in response in this study MD simulations of model nanocolloidal particles in solution at infinite dilution have been undertaken. Simulations were carried out in the absence of gravity with both smooth and atomistically rough particles with variable diameters compared to those of the solvent molecule. A preliminary study of the present MD model was reported recently which focused on the technical aspects of the cluster construction and system-size effects (Heyes *et al* 1996). In this work these techniques have been used to compute the translational and rotational diffusion coefficients, and their dependence on colloidal particle size and the ratio of the mass density of the colloidal particle to that of the bulk solvent.

## 2. Computational details

The MD computer simulations had one model colloidal particle and many solvent molecules in a cubic simulation box. First we consider the law of interaction between the molecules.

### *2.1. Solvent molecules*

The solvent–solvent molecule interactions were the purely repulsive Weeks–Chandler–Anderson, WCA, potential (Weeks *et al* 1971) which is a potential formed out of the repulsive part of the Lennard-Jones, LJ, potential (Hansen and McDonald 1986) shifted upwards by the minimum energy, $\epsilon$, and truncated at the potential minimum $r_m = 2^{1/6}\sigma_s$, where $\sigma_s$ is the diameter of the particle. One of the advantages of the WCA potential is that it is short ranged and therefore the temporal evolution of the solvent can be computed relatively efficiently. For the system sizes considered here, almost all of the computer time is spent in generating the trajectories of the solvent molecules. With available computing

facilities it was not possible to model a more realistic model solvent, such as a Lennard-Jones liquid. The solvent number density $\rho_s = N\sigma_s^3/V$ for $N$ molecules in a volume $V$. Two types of model colloidal particle were considered.

### *2.2. Smooth colloidal particle*

In the first type, the nanoparticle had a single centre of interaction with the solvent molecules. The potential originated from the centre of the model colloidal particle. The WCA potential was modified to reflect the volume of the colloid particle (Rull *et al* 1989):

$$u(r) = \begin{cases} 4\epsilon\left(\left(\dfrac{\sigma_s}{r-\alpha}\right)^{12} - \left(\dfrac{\sigma_s}{r-\alpha}\right)^{6}\right) + \epsilon & \text{for } r \leqslant r_m \\ 0 & \text{for } r > r_m. \end{cases} \tag{1}$$

This model for the colloid has been used by us before in previous publications—for example, Nuevo *et al* (1995). The advantage of this analytic form is that it is a simple generalization of the solvent–solvent potential. The central potential field is shifted out a further radial distance, $\alpha$, while retaining the same curvature as between two solvent molecules (i.e., the case when $\alpha = 0$) which minimizes any numerical algorithmic errors in updating the particle positions. The cut-off separation, $r_m$, for this potential is $r_m = \alpha + 2^{1/6}\sigma_s$. An alternative procedure would have been to have used the WCA form with the combining rules $\sigma_{cs} = (\sigma_c + \sigma_s)/2$ where $\sigma_c$ is the diameter of the colloidal particle. The cut-off is then $r_m = 2^{1/6}\sigma_{cs}$. A comparison between these two potential forms allows us to relate $\alpha$ to an equivalent core diameter for the colloidal particle. That is, $\sigma_{cs} \approx \sigma_s + \alpha$, which gives $\sigma_c \approx \sigma_s + 2\alpha$.

The mass of the model colloidal particle, $M_c$, ranged through $0.3 < M_c/m < 4.0$, where $m$ is the mass of the solvent molecule, which enabled us to explore the effects of the relative densities of the model nanocolloid and the bulk solvent, i.e., $\sim M_c\sigma_s^3/\sigma_c^3 m\rho_s$.

### *2.3. Rough colloidal particle*

A more realistic representation of a colloidal particle is to include the atomistic detail. Such a procedure has been used before in simulation studies (e.g., Bajan-Nunez and Dickinson 1994). The second type of colloidal particle was atomistically discrete and in the form of a cluster of atoms that was near-spherical. The cluster had $N_{clus}$ atoms and it was able to exchange energy and momentum with its surroundings in a realistic fashion. Also, as the colloidal particle was atomistically rough it could exhibit rotational relaxation (unlike the smooth model colloidal particle) on the fluid timescale by interaction and exchange of momentum and energy with the solvent molecules. The solid amorphous cluster was assembled out of atoms interacting via the Lennard-Jones potential,

$$\phi(r) = 4\epsilon_{\mathrm{LJ}}\left(\left(\frac{\sigma}{r}\right)^{12} - \left(\frac{\sigma}{r}\right)^{6}\right) \tag{2}$$

without truncation and using an extremely large value of the well-depth energy compared to that characterizing the solvent–solvent interaction energy, namely, $\epsilon_{\mathrm{LJ}}/\epsilon = 15$. All of the simulations were carried out at a reduced temperature $k_{\mathrm{B}}T/\epsilon = 1$. The extreme depth of the cluster atom–atom interaction within the cluster was principally to eliminate surface melting and loss of cluster atoms to the solvent during the simulation, which can easily happen for smaller values because of the reduced coordination number in the surface region. The reduced units used here are those characterizing the solvent, i.e., $m = \epsilon = \sigma_s = 1$. The

cluster atoms and the solvent molecules had the same core diameter, i.e., $\sigma = \sigma_s$. The extremely deep LJ potential (compared with $k_BT$) held the atoms tightly together. The simulation was carried out without the usual $2.5\sigma_{LJ}$ truncation distance so that each atom was allowed to interact with all others in the cluster. These factors ensured that the cluster would not break up during the simulation and would retain the same geometry. Also, importantly, this removed any possibility of plastic deformation and any resulting sudden change in energy of the cluster during a simulation, which could have affected the dynamics of the cluster through the solvent.

The cluster was created from all of the atoms in a sphere placed around an arbitrary fluid atom taken from an equilibrated liquid-state simulation configuration. This procedure had the advantage that it ensured that there was a near-spherical amorphous starting state for the cluster. The atoms captured within this sphere were then rapidly 'frozen' in essentially the same position by introducing the strongly attractive LJ interaction between the atoms as discussed above. The average number density of the atoms in the cluster so formed was similar to that of the solvent at $\rho \simeq 0.9$. The mass of each LJ atom on the cluster, $m_c$, ranged through $0.2 < m_c/m < 4.0$ which again enabled us to explore the effects of the relative mass densities of the cluster and the solvent particles, albeit over a limited density range. In this case the mass of the model nanoparticle was $M_c = N_{clus}m_c$. Typically the masses of the rough model colloidal particles were higher than those formed using the smooth-particle method.

It was important that the structure of the cluster was chosen to model a rough sphere that did not rearrange on timescales important for the dynamical features of interest here. The clusters of rapidly 'frozen' particles were in a glassy state rather than being micro-crystalline. Each cluster was probably not in its lowest free-energy state. After some time (presumably long) it is conceivable that a fluctuation might cause a cluster to reorganize into another local minimum with a slightly different structure. From the radial density distribution functions from the centre of the cluster calculated at various times during the simulation, we saw no evidence of such a reorganization during the simulations, as we would expect as the effective reduced temperature for the atoms in the cluster was $\epsilon/15k_B$. Nevertheless thermal equilibration was rapid on the timescale of the simulation and the cluster atoms soon achieved the temperature of the solvent. There has been much interest in the stability of small rare-gas cluster microstructures (e.g., Beck *et al* 1987, Stillinger and Stillinger 1990), although for the purposes of this work, the internal structure was not of great significance—as long as it did not rearrange during the simulation.

Clusters containing up to 256 atoms were simulated where the total number of atoms in the system, $N$, was 8000 in all cases. The larger the cluster, the larger the number of solvent molecules has to be to remove significant finite-size effects. Finite-$N$ effects are statistically insignificant for systems containing above about $N = 8000$ solvent molecules and a cluster consisting of about 100 atoms (Heyes *et al* 1996). The solvent density is approximated by that of the original fluid prior to creating a cluster from $N_{clus}$ of the solvent molecules (atoms). Although there is some contraction of the space occupied by the $N_{clus}$ atoms, the effect on the density of the remaining solvent molecules is negligible for $N = 8000$ or higher.

The volume of the nanocolloids created by the above procedure is not known in advance. The size of the cluster can be estimated from the mean square radius, $r_m^2$, which is readily computed as a time average:

$$r_m^2 = \left(\sum_{i=1}^{N_{clus}} m_i \boldsymbol{r}_i^2\right) \Big/ \left(\sum_{i=1}^{N_{clus}} m_i\right) \tag{3}$$

where $\boldsymbol{r}_i$ is the vector position of atom $i$ from the centre of mass of the cluster. The mass of each atom, $m_i$, was set equal to the same value, $m_c$, in this study. The effective outer radius $a$ of a homogeneous sphere is related to the mean square radius by integration and assuming a homogeneous mass distribution:

$$a = (5r_m^2/3)^{1/2}. \tag{4}$$

The effective diameter of the cluster is $\sigma_c = 2a$. The moment of inertia of the sphere, $I = 2M_c a^2/5$ (Spiegel 1967) and therefore $I = 2r_m^2 M_c/3$. For clusters with $N_{clus} = 20, 50, 120, 144$ and 256 we have, using equation (4) and the values of $r_m^2$ obtained from the simulations, diameters for the clusters $\sigma_c/\sigma = 3.3, 4.5, 6.1, 6.4$ and 9.1, respectively.

**Table 1.** Summary of some of the principal properties from the $N_{clus} = 256$ rough-colloidal-particle simulations. Key: $\rho_s$, solvent density; $N_{clus}$, number of LJ atoms in the cluster; $N_T$, number of time steps in the production simulation; $r_m^2$ is the mean square radius calculated from equation (3); $D_{trans}$(clus) is the translational self-diffusion coefficient of the cluster; $D_{trans}$(solv) is the translational self-diffusion coefficient of the solvent molecules; $D_{rot}$(clus) is the rotational diffusion coefficient of the cluster from equation (10); $\eta_s$ is the solvent shear viscosity obtained from the appropriate Green–Kubo formula (Hansen and McDonald 1986); $\tau_\omega$ is the angular velocity relaxation time from equation (8). $m_c/m$ is the ratio of the mass of an atom in the LJ cluster (all the same) and $m$ is the mass of a WCA solvent molecule. The self-diffusion coefficients, relaxation times and shear viscosity are estimated to be uncertain to typically ±5%.

| $\rho_s$ | $N_{clus}$ | $m_c/m$ | $N_T$ /$10^3$ | $\langle r_m^2 \rangle$ | $D_{trans}$(clus) /$10^{-2}$ | $D_{trans}$(solv) | $D_{rot}$(clus) /$10^{-3}$ | $\eta_s$ | $\tau_\omega$ |
|---|---|---|---|---|---|---|---|---|---|
| 0.7 | 256 | 0.2 | 3225 | 9.0231 | 0.810 | 0.132 | 0.657 | 0.795 | 0.226 |
| 0.7 | 256 | 0.2 | 3725 | 9.0211 | 0.834 | 0.137 | 0.722 | 0.799 | 0.230 |
| 0.7 | 256 | 1.0 | 610 | 9.0466 | 0.769 | 0.133 | 0.580 | 0.817 | 1.121 |
| 0.7 | 256 | 1.0 | 2855 | 9.0399 | 0.653 | 0.131 | 0.721 | 0.800 | 0.998 |
| 0.9 | 256 | 0.2 | 1510 | 9.1018 | 0.219 | 0.0467 | 0.198 | 2.81 | 0.0656 |
| 0.9 | 256 | 1.0 | 1135 | 9.0934 | 0.200 | 0.0470 | 0.181 | 2.99 | 0.288 |
| 0.9 | 256 | 5.0 | 2780 | 9.0894 | 0.177 | 0.0474 | 0.213 | 2.83 | 1.611 |
| 1.0 | 256 | 1.0 | 1090 | 9.0565 | 0.0585 | 0.0211 | 0.0728 | 7.69 | 0.104 |
| 1.0 | 256 | 5.0 | 960 | 9.0571 | 0.0564 | 0.0216 | 0.0729 | 7.46 | 0.522 |
| 1.0 | 256 | 5.0 | 1770 | 9.0567 | 0.0565 | 0.0215 | 0.0710 | 7.45 | 0.533 |

### *2.4. Technical details of the simulations*

The computations were made faster using link cells to construct a neighbourhood table of near interactions (Fincham and Heyes 1985). The integration of the equations of motion was carried out using the Verlet algorithm with periodic velocity rescaling at solvent reduced densities $\rho_s = N\sigma^3/V$ in the range 0.6–0.9 and at a reduced temperature of $k_B T/\epsilon = 1.0$, where $k_B$ is Boltzmann's constant. The time step was $h = 0.005\sigma(m/\epsilon)^{1/2}$ and the simulations were carried out typically for $\simeq 10^6$ time steps. The time correlation functions were evaluated using the fast Fourier transform, FFT, method (Fincham and Heyes 1985). The use of the FFT method was crucial to the feasibility of these simulations, as dynamical processes took place on all timescales up to $80\sigma(m/\epsilon)^{1/2}$ for the largest clusters considered, ranging from rapid solvent and cluster angular momentum relaxation on the $(1–2)\sigma(m/\epsilon)^{1/2}$ timescale to much slower cluster reorientational relaxation typically up to at least the $80\sigma(m/\epsilon)^{1/2}$ timescale depending on cluster size. The simulations were

continued until adequate statistics was obtained for the modelled quantities (principally the translational and rotational diffusion coefficients of the nanoparticles). The length of each correlation function was such that it had statistically decayed to zero well within the period. The model nanocolloidal clusters typically moved many times their mean diameters in a simulation. This distance can be estimated from $\sim(6Dt_{sim})^{1/2}$ where $t_{sim}$ is the duration of the simulation and $D$ is the translational self-diffusion coefficient of the nanocolloid. For the systems and solvent states given in table 1 we have, for the $N_{clus} = 256$ rough clusters, displacements during the 'production' phase of the simulation of $3, 1.5$ and $0.5$ cluster diameters at solvent densities of $\rho_s = 0.7, 0.9$ and $1.0$ respectively. The displacements were even larger for the smaller nanocolloids.

Even though we were nominally considering a system at infinite dilution, as there was only one colloidal particle in the cell, the system was surrounded by periodic images of itself. The solvent hydrodynamic disturbances caused by the model colloidal particle will re-enter the cell via the periodic boundary condition construction and affect the colloidal particle's dynamics in an unpredictable manner. Hydrodynamic interactions are long ranged and, unless the system size is large when compared with the colloidal particle, the interactions of the particle with its own images could lead to serious artefacts in its dynamical evolution. We therefore had to use a sufficiently large number of solvent molecules to bring any finite-$N$ effects to a tolerable and practicable minimum. In our previous study we made an extensive assessment of these effects by carrying out simulations with varying numbers of solvent molecules. We found for colloidal particles in the diameter range used here that $\simeq$8000 solvent molecules were sufficient to eliminate any noticeable size effects on the translational self-diffusion coefficients. We expect the size effects to be even smaller for rotational self-diffusion, as the range of the hydrodynamical disturbance caused by rotational motion is known to be less than that arising from translational motion. Based on this evidence, the solvent system is large enough and the cluster particle is still sufficiently small that any hydrodynamic (long-range) interference between the cluster images can be considered as irrelevant, at least as far as the values of the self-diffusion coefficients is concerned. For clusters containing $N_{clus}$ atoms then there were $N - N_{clus}$ solvent atoms, where $N = 8000$. For solvent reduced number densities $\rho_s = 0.7$–$0.9$, the corresponding cubic simulation cell sides were $(23$–$21)\sigma$ respectively.

## 3. Theoretical background of rotational relaxation

For the rough model colloidal particles, the orientational dynamics can be described in a compact way using the family of time correlation functions (Clarke 1978)

$$C^l(t) = \langle P_l(\boldsymbol{u}(t) \cdot \boldsymbol{u}(0))\rangle \tag{5}$$

where $\boldsymbol{u}$ is an arbitrary unit vector embedded in the cluster and passing through its centre, and $P_l$ is the $l$th-order Legendre polynomial. The first rank ($l = 1$) is related to the infrared absorption spectrum, the second rank ($l = 2$) to the Raman scattering spectrum, and all ranks contribute to inelastic neutron scattering. More fundamental correlation functions are the angular velocity autocorrelation function (ACF) in the principal-axis frame of the cluster, $\boldsymbol{\omega}$,

$$C_\omega(t) = \langle \boldsymbol{\omega}(0) \cdot \boldsymbol{\omega}(t)\rangle \tag{6}$$

and the torque ACF which however are not directly measurable by experiment. By analogy with the translational diffusion coefficient it is possible to define the time-dependent

rotational diffusion coefficient, $D_{rot}(t)$,

$$D_{rot}(t) = \frac{kT}{I}\int_0^t \left(1 - \frac{s}{t}\right) C_\omega(s)\ \mathrm{d}s = \frac{kT}{I}\tau_\omega \tag{7}$$

where $I$ is the moment of inertia. The rotational diffusion coefficient, $D_{rot}$, is the limit, $D_{rot}(t \to \infty)$. The fact that the clusters are geometrically rigid on an atomistic scale and essentially spherical enables their rotational motion to be readily characterized using a *single* rotational diffusion coefficient, $D_{rot}$. The time-dependent angular velocity relaxation time, $\tau_\omega(t)$, is derived from $C_\omega(t)$:

$$\tau_\omega(t) = \int_0^t \left(1 - \frac{s}{t}\right) \frac{C_\omega(s)}{C_\omega(0)}\ \mathrm{d}s. \tag{8}$$

The rotational relaxation time $\tau_\omega = \tau_\omega(t \to \infty)$. The $C_\omega$ and $C^l$ are connected via the cumulant expansion (Tildesley and Madden 1983)

$$\ln(C^l(t)) = -l(l+1)\frac{kT}{I}\int_0^t (t-s)C_\omega(s)\ \mathrm{d}s. \tag{9}$$

This relation gives the correct limits. In the short-time limit $t \ll \tau_\omega$, $C_\omega(t) \simeq 1$ and hence

$$\ln(C^l(t)) \simeq -l(l+1)kTt^2/2I \qquad \text{or} \qquad C^l(t)_{t\to 0} \simeq 1 - l(l+1)kTt^2/2I$$

so the short-time limit is in accord with the free-rotor model. In the long-time limit, $t \gg \tau_\omega$,

$$\ln(C^l(t)) \simeq -l(l+1)kT\tau_\omega t/2I \qquad \text{or} \qquad C^l(t)_{t\to\infty} \simeq \exp(-l(l+1)D_{rot}t)$$

where $D_{rot} = kT\tau_\omega/I$. On times longer than the inertial relaxation timescale for $l = 1$,

$$D_{rot} = -\frac{1}{2}\lim_{t\to\infty}\frac{\mathrm{d}}{\mathrm{d}t}\ln(C^1(t)). \tag{10}$$

Therefore we have two methods for extracting $D_{rot}$ for the model colloidal particle, via $C^l$ or $C_\omega$. The reorientational relaxation time, $\tau_u$, for the $P_1$-term in equation (5) is obtained from $\tau_u = 1/2D_{rot}$.

Two independent procedures were used to define the unit vector $\boldsymbol{u}$. One was to calculate the principal coordinate system of the starting configuration of the colloidal cluster and then evolve one of these unit vectors with time using the quaternion technique used by Heyes *et al* (1996) assuming a rigid structure, which is a good approximation for these geometrically rigid clusters. The second (simpler to implement) approach was to find the two LJ atoms that were the furthest apart in the cluster, and to use their separation vector as the basis for the unit vector.

## 4. Results and discussion

### *4.1. Structure*

The number density profile taken from the centre of an 120-atom rough cluster in a fluid at solvent density $\rho_s = 0.9$ is shown in figure 1. It is seen to have a highly structured region at small distances from the centre, $r$, arising from the atoms within the cluster as they are essentially 'frozen' in their original liquid-state positions. The atoms are mainly distributed into three well defined shells/bands. As the bands are quite structured and broad, it would be difficult to discern any regular structure (e.g., FCC-like or some other well known regular cluster structure). Figure 1 also shows that the density of the cluster (via $m_c/m$ values chosen in the range 0.2–4.0) had no noticeable effect on these number density profiles, as would be expected for a classical model. The solvent number density profiles exhibited density

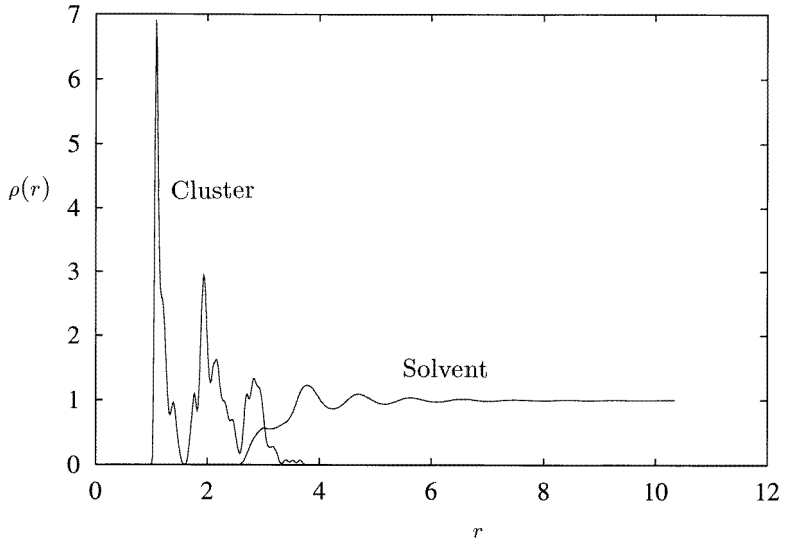


**Figure 1.** Number density profiles of atoms in the $N_{clus} = 120$ rough cluster and the solvent taken from the centre of the cluster at the solvent number density $\rho_s = 0.9$. The density profiles are normalized with respect to the bulk solvent number density. The profiles for a range of values $0.2 \leqslant m_c/m \leqslant 4.0$ are indistinguishable in this figure.

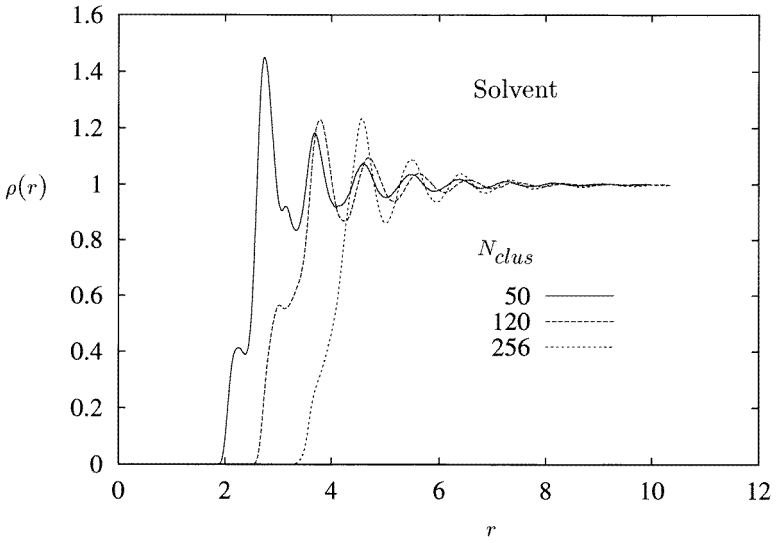


**Figure 2.** Density profiles of the solvent molecules around rough clusters of variable size. The values of $N_{clus}$ are given in the figure. The bulk solvent density was $\rho_s = 0.9$, and the density profiles presented are normalized with respect to the bulk density.

oscillations next to the nanocolloid's surface that gradually decayed away with distance radially from the centre of the cluster. These indicate the presence of 'layers' of solvent cages around the nanocolloid. At larger $r$ the solvent number density profile is uniform, approaching that of the bulk fluid. The oscillations in solvent number density become

more pronounced and long ranged with increasing $\rho_s$. Figure 2 shows the solvent radial density profile arising from rough clusters of different sizes. There is evident significant overlap between the cluster and solvent number density distributions, which ensured a strong coupling between the trajectories of the solvent and cluster atoms with the possibility of generation of substantial rotational motion of the cluster. The $m_c/m$ value chosen in the range 0.2–4.0 had no noticeable effect on these solvent number density profiles.

### *4.2. Centre-of-mass motion*

*4.2.1. Time correlation functions.* The normalized force and velocity autocorrelation functions

$$C_F(t) = \frac{\langle \boldsymbol{F}(t) \cdot \boldsymbol{F}(0) \rangle}{\langle \boldsymbol{F}^2(0) \rangle} \tag{11}$$

$$C_V(t) = \frac{\langle \boldsymbol{v}(t) \cdot \boldsymbol{v}(0) \rangle}{\langle \boldsymbol{v}^2(0) \rangle} \tag{12}$$

respectively were calculated, as were the time-dependent self-diffusion coefficients (Hansen and McDonald 1986)

$$D(t) = (1/3) \int_0^t (1 - \tau/t) \langle \boldsymbol{v}(\tau) \cdot \boldsymbol{v}(0) \rangle \, \mathrm{d}\tau. \tag{13}$$

In practice the time correlation functions were integrated out to sufficiently long times ($t$) that the $1-\tau/t$ term had an insignificant effect on the value of the self-diffusion coefficient, $D$ (i.e., $D(t)$ in the $t \to \infty$ limit).

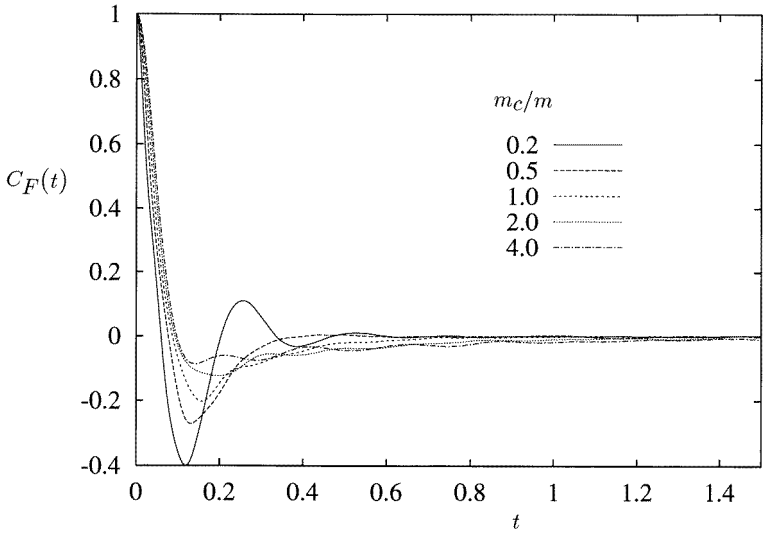


**Figure 3.** Normalized cluster force autocorrelation functions, $C_F(t)$, for the $N_{clus} = 120$ rough cluster in a $\rho_s = 0.9$ solvent with mass ratios in the range $0.2 \leqslant m_c/m \leqslant 4.0$.

For the clusters the quantities $\boldsymbol{F}$ and $\boldsymbol{v}$ refer to the net (i.e., centre-of-mass) force and velocity of the cluster. The self-diffusion coefficients show a decrease with increasing density which is typical fluid behaviour. In figure 3, the nanocolloid force autocorrelation functions (FACF) obtained from the 120-atom clusters at $\rho = 0.9$ across a wide $m_c/m$

range are presented. (The ratio $m_c/m$ is approximately the ratio of the mass densities of the nanocolloidal particle and the bulk solvent mass density, as the particle number densities of these are quite similar.) As the mass density of the cluster decreases, the FACF shows increasing evidence of 'backscattering' behaviour, which is also reflected in the velocity autocorrelation functions. As the density of the solute particle decreases, the FACF demonstrates that it oscillates within its cage with increasing frequency.

There has been increasing interest in recent years in establishing the statistical mechanical basis of the velocity relaxation of single spherical colloidal particles in a solvent (e.g., Hinch 1975, Weitz *et al* 1989, Espagñol and Zúñiga 1995), and it is still far from a solved problem. Interpretation and rationalization of this behaviour has been in terms of several key relaxation times and their relative magnitudes. There is a characteristic relaxation time of hydrodynamic relaxation of the solvent from disturbances on the scale of the colloidal particle caused by the colloidal particle, $\tau_s \approx \sigma_c^2/\eta_{kin}$ where $\eta_{kin} = \eta_s/m\rho_s$ is the kinematic shear viscosity and $\eta_s$ is the shear viscosity. On the basis of the velocity Langevin equation, we also have the relaxation time of the velocity of the colloidal particle, $\tau_v \sim M_c/\zeta$ where $\zeta \sim \eta_s\sigma_c$ is Stokes's friction coefficient. Therefore $\tau_s/\tau_v \sim m\rho_s\sigma_c^3/M_c$ which is also the ratio of the mass density of the bulk solvent to that of the colloidal particle alone. In the limit of $\tau_s/\tau_v \ll 1$ all of the dynamical processes are Markovian, and the Langevin and Fokker–Planck equations can be assumed valid. In this limit the colloidal particle's velocity relaxation is exponential in time with a relaxation time of $\tau_v$. We see that this will only happen if the mass density of the colloidal particle is much greater than that of the bulk fluid (i.e., if $m/M_c \to 0$). This is, in principle, feasible in a simulation but not of great practical use because such colloidal particles would sediment under gravity (if greater than about a micron in size). In our simulations we were considering the $\tau_s \sim \tau_v$ regime and we therefore do not have a clear separation of these two timescales, and the velocity Langevin equation and the Fokker–Planck equation are not valid in this situation. The 'short-time' departure from the Langevin prediction for $D(\tau)$ has been observed for real colloidal liquids at infinite dilution using diffusive wave spectroscopy (DWS) (e.g., Zhu *et al* 1992). The overlap of these timescales and the coupling of these two dynamical processes (solvent and colloid particle velocity relaxation) can be treated by assuming that the fluid obeys fluctuating hydrodynamics and the colloid the generalized Langevin equation, out of which emerges a long-time relaxation of the velocity autocorrelation function as $\sim k_{\mathrm{B}}T/2\pi^2\sigma_c^3\rho_s t^{3/2}$.

Most of our simulations were carried out in the $\tau_s \sim \tau_v$ region, so neither an algebraic law decay (exponent 3/2) nor an exponential decay would be expected. In fact, due to the statistical noise and the relatively short time range over which the correlation function is known accurately, it is difficult to distinguish between these two analytic forms anyway. An example intended to reveal the possibility of exponential relaxation is presented in figure 4, which shows a log–linear plot of the nanocolloid's velocity autocorrelation functions (VACF) obtained from the 120-atom structured clusters at $\rho = 0.9$ for $0.2 < m_c/m < 4.0$. It does show that as the density of the particle increases, the VACF tends to the predicted exponential form.

*4.2.2. Diffusion coefficients.* Despite the sensitivity of the form of the force and velocity autocorrelation functions to the nanocolloid mass density there is little corresponding variation in the value of the self-diffusion coefficient at liquid-like solvent densities. There is a noticeable gradual decrease in $D$ with increasing colloid mass at a solvent density $\rho_s = 0.7$ but no statistically significant variation at $\rho_s = 0.9$. This may be seen in figure 5, which

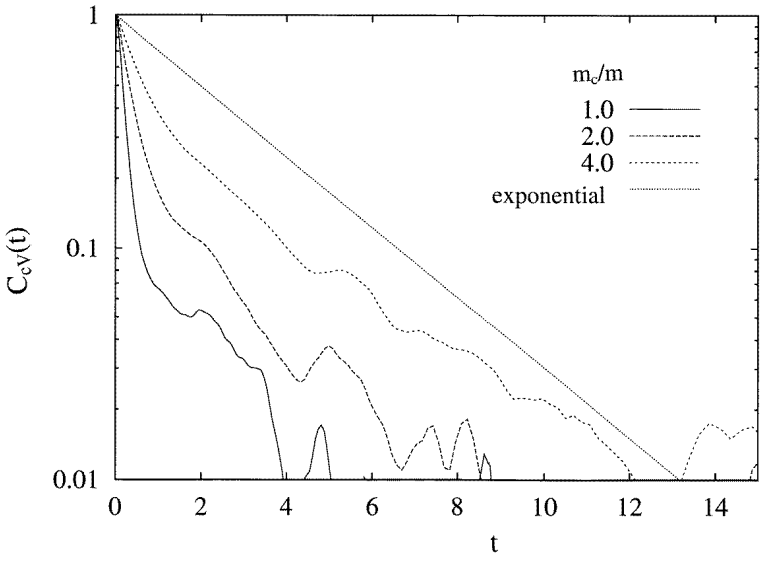


**Figure 4.** A log–linear plot of the velocity autocorrelation functions for the systems of figure 3. The straight line is for $\exp(-t/\tau_v)$ where $\tau_v = M_c/3\pi\eta_s\sigma_c$. Using $\sigma_c = 6.0$ and $\eta_s = 2.95$ we have $\tau_v = 0.71 m_c/m$ for the largest density considered. The straight line corresponds to $m_c/m = 4.0$.

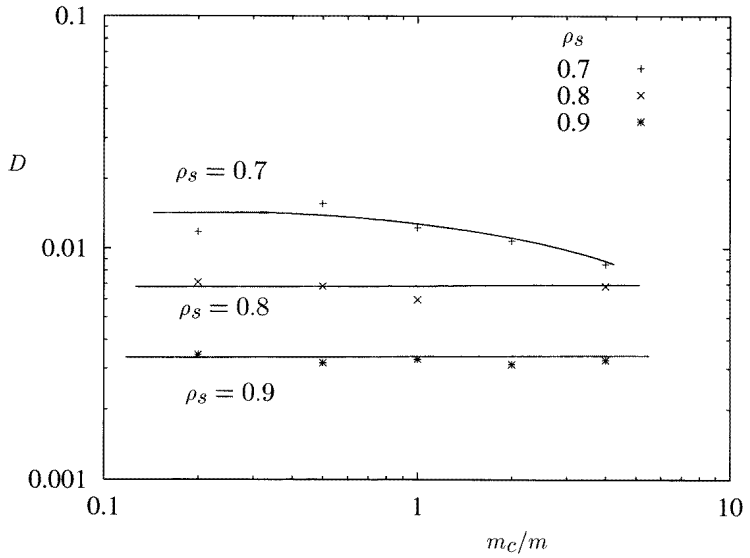


**Figure 5.** The colloid mass dependence of the self-diffusion coefficients for an $N_{clus} = 120$ rough cluster at three values for the solvent density.

shows the $m_s/m$ dependence of $D$ for the clusters of $N_{clus} = 120$ rough particles at various solvent densities. Table 1 gives simulation data for clusters of $N = 256$ particles, and it also reveals that there is a decrease with $m_c/m$ in $D$ for a solvent number density of $\rho = 0.7$

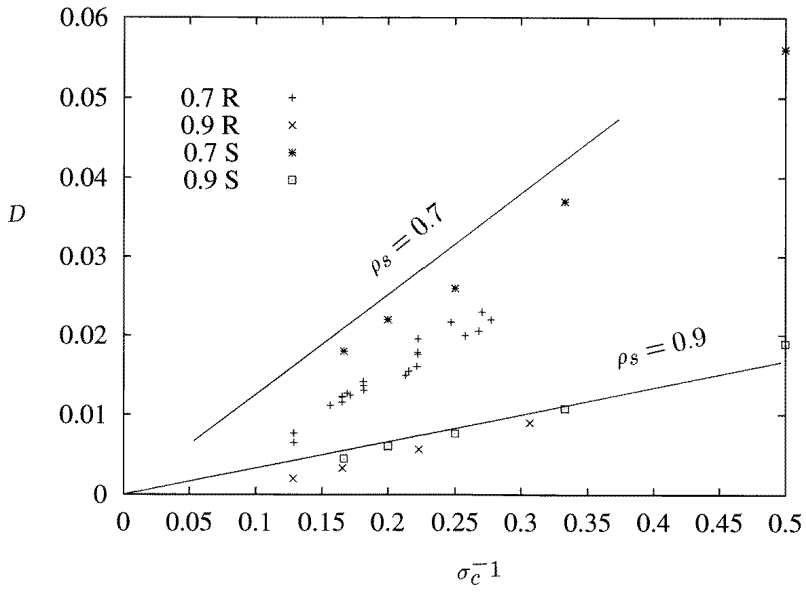


**Figure 6.** The dependence of the translational self-diffusion coefficient on $\sigma_c^{-1}$ for two values of the solvent density distinguishing between the behaviour of smooth and rough spheres. The lines are the prediction of the Stokes–Einstein relationship using stick boundary conditions and based on the shear viscosity of 0.84 at $\rho_s = 0.7$ and 3.05 at $\rho_s = 0.9$ obtained using the Green–Kubo linear response method (Hansen and McDonald 1986). The masses for both types of cluster are chosen in the range where the diffusion coefficients are mass independent ($M_c/m = 1$ for the smooth nanocolloid and $m_c/m = 1$ for the rough cluster.)

in the range where the density of the solute particle is greater than that of the solvent. The mass dependence for the $N = 256$ cluster seems to be somewhat more pronounced at all densities than for the $N = 120$ particles, which could be a finite-size effect originating in the 'backflow' of solvent generated by the diffusion of the colloidal particle. As the total translational momentum of the cell is equal to zero at all times, the translation of a massive particle will induce a counter-current of solvent molecules in the opposite direction which will reduce the self-diffusion coefficient of the colloidal particle. It is interesting that table 1 shows that the rotational diffusion coefficient does not show a corresponding mass dependence for the $N_{clus} = 256$ cluster systems, possibly because there is no conservation of rotational angular momentum in the simulation system. Previous simulations of massive (but much smaller) solute particles in a solvent have revealed a relative insensitivity of the translational diffusion coefficient to the mass of the cluster (or equivalently the ratio of the colloidal particle density to that of the solute molecule $\rho_c/\rho_s$) (Rull *et al* 1989). Perhaps surprisingly, the density of the nanocolloidal particle has virtually no effect on the value of the self-diffusion coefficient at liquid-like solvent densities. This is in marked contrast to the situation prevailing in dilute gases, where the self-diffusion coefficient is strongly mass dependent ($\sim M^{-1/2}$). According to the Stokes–Einstein expression, the mass of the particle is not expected to affect the diffusion coefficient. The inertia of the particle would be expected to have an influence when the ideal of short Brownian steps does not apply and longer steps between 'collisions' become significant (i.e., the mean free path is no longer infinitesimal compared to the diameter of the solvent molecule). This gradual change in dynamics at progressively lower solvent number density is responsible for the transition

to dilute-gas-limit behaviour in the self-diffusion coefficient and the increasing sensitivity to the value of the mass of the colloidal particle. The diffusion coefficient is, however, sensitive to solvent bulk number density and to the size of the solute particle, and therefore it would appear to be the mean free path of the colloidal particle in its collisions with the surrounding solvent molecules that largely determines the value of $D$.

The classical solution for the dependence of $D$ on sphere diameter and solvent viscosity is the Stokes–Einstein (SE) relationship,

$$D = \frac{k_B T}{n\pi \eta_s \sigma_c} \tag{14}$$

where $n = 3$ for stick and $n = 2$ for slip boundary conditions, and $\eta_s$ is the solvent viscosity. A plot of $D$ against $\sigma_c^{-1}$ for the smooth and rough spheres is given in figure 6 for two solvent densities ($\rho_s = 0.7$ and $\rho_s = 0.9$). The smooth colloidal particles fall closer to the classical line predicted by the SE relationship, using the Newtonian shear viscosity of the solvent obtained by the Green–Kubo method (Hansen and McDonald 1986). Within the statistical uncertainty, the $D$-values of the smooth and rough particles fall on the same line at the higher solvent density. However, at $\rho_s = 0.7$ the $D$-values of the rough particles are systematically lower than those of the equivalent-diameter smooth particle. The origin of this difference may lie in the differences in the solvent structure around the smooth and rough colloidal particles at the lower density. Figure 7 compares the density profile for $\sigma_c \simeq 6.0$ colloidal particles in the two cases for (a) $\rho_s = 0.7$ and (b) $\rho_s = 0.9$ solvent densities. The smooth particle presents a sharper boundary with the solvent, and against which layers of solvent can more effectively organize. The rough particle has a more diffuse interaction with the solvent which nevertheless could be more effective at ordering the solvent around it, embedding the model colloidal particle within a solvent cage and hence slowing down the translational diffusion to a greater extent by virtue of an enhancement of the local viscosity experienced by the particle. Despite the more pronounced radial density oscillations for the smooth colloidal particles, it is possible that the rough particle is more effectively constrained by its solvent cage. Alternatively, one could interpret the reduction in the diffusion coefficient as an increase of the effective hydrodynamic radius of the particle as a result of this cage effect (i.e., the nanoparticle 'drags' some of the solvent with it as it translates, thereby increasing its effective size). Whatever the precise cause, its consequences will probably diminish as the nanocolloid approaches micron dimensions and the ratio of the surface layer volume to colloidal particle volume diminishes. In this limit, the bulk shear viscosity of the solvent will become the relevant parameter governing the diffusion of the colloidal particle, rather than the local viscosity in the surface layer around the colloidal particle. The diffusion coefficients will start to follow the classical prediction line given in figure 6—rather than having a non-zero intercept as implied by the data in this figure.

The higher-solvent-density states (figure 7(b)) show oscillations further out in distance from the centre of the colloidal particle but are otherwise qualitatively the same as for the lower-density $\rho_s = 0.7$ state. There is more freedom for solvent reorganization around the colloidal particle for the lower solvent density, and this is possibly why the differences between the self-diffusion coefficients between rough and smooth particles are greater at $\rho_s = 0.7$. In our comparisons with the macroscopic sphere case of equation (14) we have assumed that stick boundary conditions apply in both smooth and rough cases, which is not necessarily the case. If slip boundary conditions (i.e., $n = 2$) were used in equation (14) the difference would be even greater.

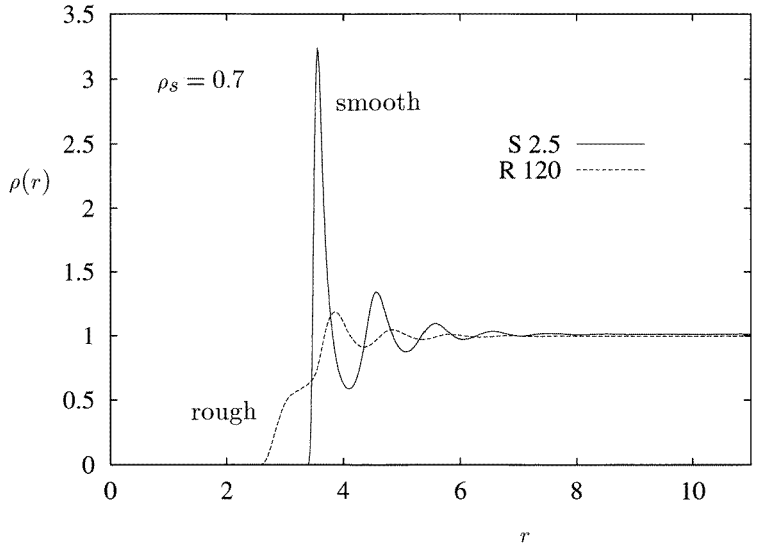


(a)

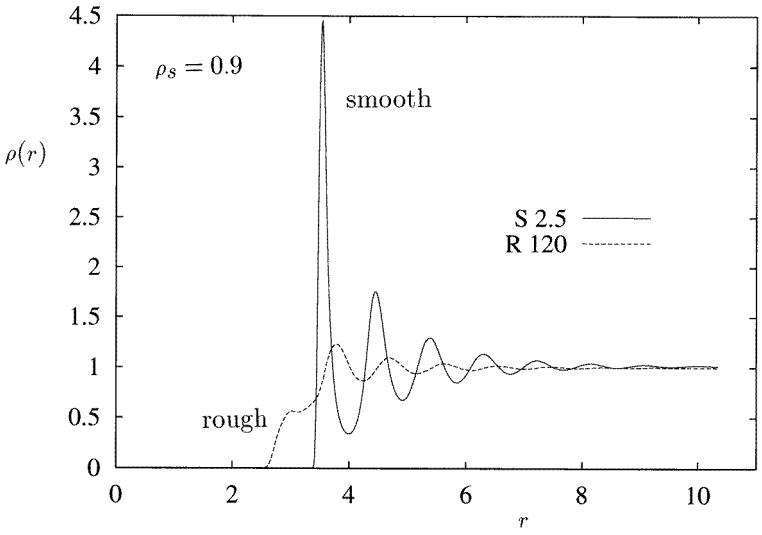


(b)

**Figure 7.** Normalized radial density profiles around smooth (S) and rough (R) $N_{clus} = 120$ colloidal particles, both with $\sigma_c \simeq 6.0$, at densities of (a) $\rho_s = 0.7$ and (b) $\rho_s = 0.9$.

### *4.3. Orientational behaviour*

We now consider the reorientational motion of the rough particle. The $P_1$-function in equation (5) and $C_\omega(t)$ were calculated for each structured nanoparticle. Typically, the $C_\omega(t)$ decayed in a monotonic fashion except for the clusters that had a low mass density and were relatively small. In these cases the $C_\omega(t)$ exhibited a shallow negative region at intermediate times (see figure 8) symptomatic of strong fluctuations in angular acceleration.

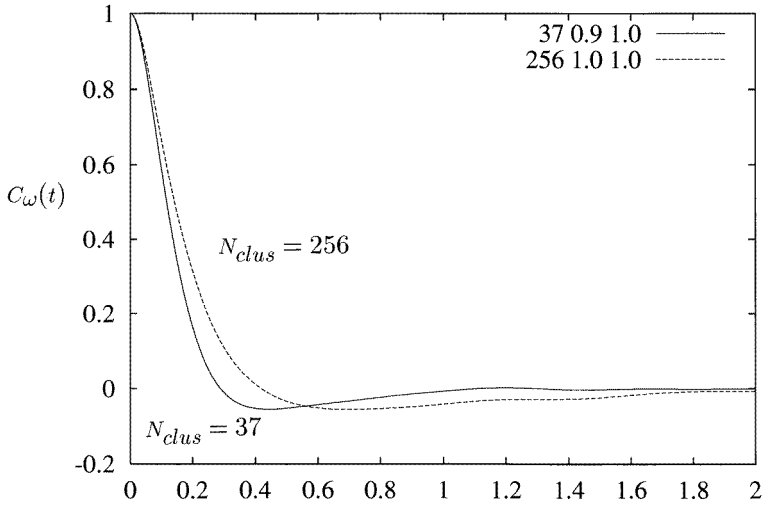


**Figure 8.** The angular velocity autocorrelation function, $C_\omega(t)$, for $N_{clus} = 37$ and $\rho_s = 0.9$, and $N_{clus} = 256$ and $\rho_s = 1.0$.

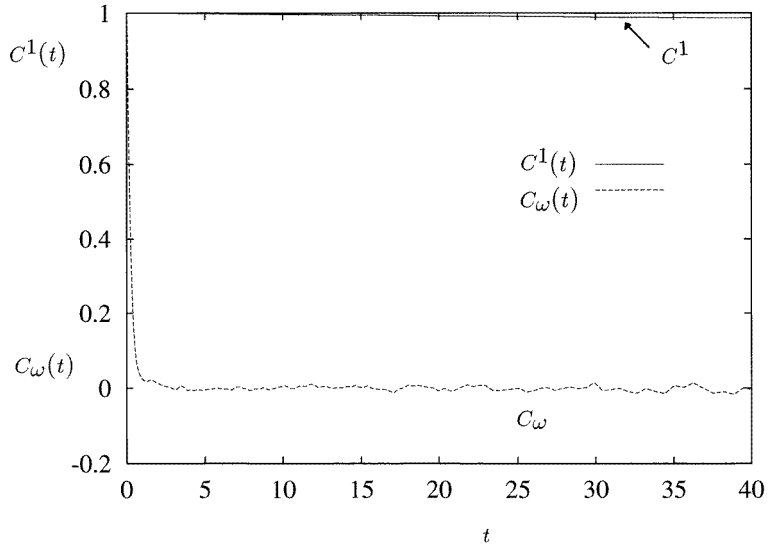


**Figure 9.** Comparison of $C_\omega(t)$ and $C^1(t)$ for the state $N = 8000$, $N_{clus} = 256$, $m_c/m = 1.0$ and $\rho_s = 0.9$.

As the size of the cluster and/or the solvent number density increased, this function decayed more slowly with time, losing the backscattering negative lobe. For the clusters studied here there is a clear separation of timescales between angular velocity relaxation and orientational relaxation as may be seen in figure 9 which shows the normalized $C_\omega(t)$ and $C^1(t)$ for a 256-atom cluster with $m_c/m = 1.0$ in a solvent at a number density of $\rho_s = 0.9$. The figure shows that there is slow reorientational relaxation ($C^1(t)$) compared with the corresponding angular velocity function $C_\omega(t)$ for all of the clusters (i.e., $\tau_u \gg \tau_\omega$). The relaxation time

$\tau_\omega$ decreases with increasing number density of the solvent whereas the $\tau_u$ increases with solvent density.

There are many models for molecular reorientation in the literature (e.g., see Clarke 1978). It is possible to make general statements about the applicability of these models to the nanoparticles studied here by comparing $\tau_u = 1/2D_{rot}$ and $\tau_\omega$ with $\tau_{rot} = (I/k_BT)^{1/2}$, the time taken for a free rotator to reorientate through one radian. For the nanocluster we have the following expression for the moment of inertia: $I = 2\langle r_m^2\rangle N_{clus}(m_c/m)/3$ which gives $\tau_{rot}/(m_c/m) = 4.6, 10.0, 20.9$ and $39.4$ for $N_{clus} = 20, 50, 120$ and $256$.

**Table 2.** Summary of the relaxation times for the simulated rough-colloidal-particle systems. Key: $\rho_s$, solvent density; $N_{clus}$, number of LJ atoms in the cluster; $I$ is the moment of inertia of the cluster obtained from the formula $I = 2\langle r_m^2\rangle N_{clus}(m_c/m)/3$ where $r_m^2$ is the mean square radius calculated from equation (3). The reorientation relaxation time, $\tau_u = 1/2D_{rot}$, and angular velocity relaxation time, $\tau_\omega$ from equation (8), are presented. With $\tau_{rot} = (I/k_BT)^{1/2}$ we define the reduced correlation times, $\tau_\omega^* = \tau_\omega/\tau_{rot}$ and $\tau_u^* = \tau_u/\tau_{rot}$; $m_c/m$ is the ratio of the mass of an atom in the LJ cluster (all the same) to that, $m$, of a WCA solvent molecule. The relaxation times are estimated to be uncertain to typically ±5%.

| $\rho_s$ | $N_{clus}$ | $m_c/m$ | $\langle r_m^2\rangle$ | $I$ | $\tau_{rot}$ | $\tau_\omega$ | $\tau_u$ | $\tau_\omega^*$ | $\tau_u^*$ |
|---|---|---|---|---|---|---|---|---|---|
| 0.90 | 20 | 0.20 | 1.60 | 4.3 | 2.1 | 0.018 | 107 | 0.009 | 51.8 |
| 0.90 | 20 | 1.00 | 1.60 | 21.3 | 4.6 | 0.084 | 130 | 0.018 | 28.3 |
| 0.90 | 20 | 4.00 | 1.60 | 85.1 | 9.2 | 0.329 | 127 | 0.036 | 13.9 |
| 0.50 | 50 | 1.00 | 3.02 | 101 | 10.0 | 1.090 | 44 | 0.109 | 4.4 |
| 0.60 | 50 | 1.00 | 3.02 | 101 | 10.0 | 0.718 | 63 | 0.072 | 6.3 |
| 0.70 | 50 | 1.00 | 3.03 | 101 | 10.1 | 0.464 | 117 | 0.046 | 11.7 |
| 0.80 | 50 | 1.00 | 3.01 | 101 | 10.0 | 0.262 | 183 | 0.026 | 18.3 |
| 0.90 | 50 | 1.00 | 3.01 | 100 | 10.0 | 0.139 | 369 | 0.014 | 36.8 |
| 1.00 | 50 | 1.00 | 2.99 | 100 | 10.0 | 0.053 | 930 | 0.005 | 93.2 |
| 0.70 | 120 | 0.20 | 5.49 | 87.9 | 9.4 | 0.163 | 325 | 0.017 | 34.7 |
| 0.70 | 120 | 0.50 | 5.49 | 220 | 14.8 | 0.386 | 319 | 0.026 | 21.5 |
| 0.70 | 120 | 1.00 | 5.49 | 439 | 21.0 | 0.820 | 313 | 0.039 | 14.9 |
| 0.70 | 120 | 2.00 | 5.49 | 878 | 29.6 | 1.318 | 329 | 0.044 | 11.1 |
| 0.70 | 120 | 4.00 | 5.49 | 1757 | 41.9 | 3.082 | 340 | 0.074 | 8.1 |
| 0.80 | 120 | 0.20 | 5.48 | 87.7 | 9.4 | 0.077 | 564 | 0.008 | 60.2 |
| 0.80 | 120 | 0.50 | 5.48 | 219 | 14.8 | 0.199 | 537 | 0.013 | 36.2 |
| 0.80 | 120 | 1.00 | 5.48 | 438 | 20.9 | 0.392 | 513 | 0.019 | 24.5 |
| 0.80 | 120 | 4.00 | 5.48 | 1754 | 41.9 | 1.775 | 511 | 0.042 | 12.2 |
| 0.90 | 120 | 0.20 | 5.47 | 87.5 | 9.4 | 0.041 | 1132 | 0.004 | 121.0 |
| 0.90 | 120 | 0.50 | 5.47 | 219 | 14.8 | 0.100 | 1140 | 0.007 | 77.1 |
| 0.90 | 120 | 1.00 | 5.47 | 437 | 20.9 | 0.185 | 1191 | 0.009 | 57.0 |
| 0.90 | 120 | 2.00 | 5.47 | 875 | 29.6 | 0.372 | 1214 | 0.013 | 41.1 |
| 0.90 | 120 | 4.00 | 5.47 | 1749 | 41.8 | 0.781 | 1166 | 0.019 | 27.9 |
| 0.70 | 256 | 0.20 | 9.02 | 308 | 17.5 | 0.230 | 692 | 0.013 | 39.4 |
| 0.70 | 256 | 1.00 | 9.04 | 1543 | 39.3 | 0.998 | 693 | 0.025 | 17.6 |
| 0.90 | 256 | 0.20 | 9.10 | 311 | 17.6 | 0.066 | 2523 | 0.004 | 143.1 |
| 0.90 | 256 | 5.00 | 9.09 | 7756 | 88.1 | 1.611 | 2345 | 0.018 | 26.6 |
| 1.00 | 256 | 5.00 | 9.06 | 7729 | 87.9 | 0.522 | 6861 | 0.006 | 78.0 |

These are typically short compared to $\tau_u$ but long compared to $\tau_\omega$. Defining the following normalized relaxation times: $\tau_\omega^* = \tau_\omega/\tau_{rot}$ and $\tau_u^* = \tau_u/\tau_{rot}$, we have, typically, $\tau_\omega^* \ll 1$ and $\tau_u^* \gg 1$ which corresponds to so-called small-step diffusion and is consistent with the wide separation between the relaxation timescales $C_\omega(t)$ and $C^1(t)$ observed for example in figure 9. (Actually, it is the torque autocorrelation function that is usually used to establish the different types of orientational relaxation behaviour. As this has a shorter relaxation time, $\tau_T$, than that of the angular velocity, the trend will be even more pronounced than that adequately revealed using $\tau_\omega$.) Table 2 shows that $\tau_\omega^*$ and $\tau_u^*$ are sensitive to nanocolloid mass density, size and solvent number density. As the mass density of the cluster increases, $\tau_\omega^*$ increases and $\tau_u^*$ decreases, indicative of greater persistence in angular velocity and longer-lived 'collision' events ('extended diffusion'). A similar trend occurs as the solvent number density decreases. Therefore the small-step limiting diffusion behaviour is most readily achieved at high solvent number densities, low cluster masses and for larger clusters.

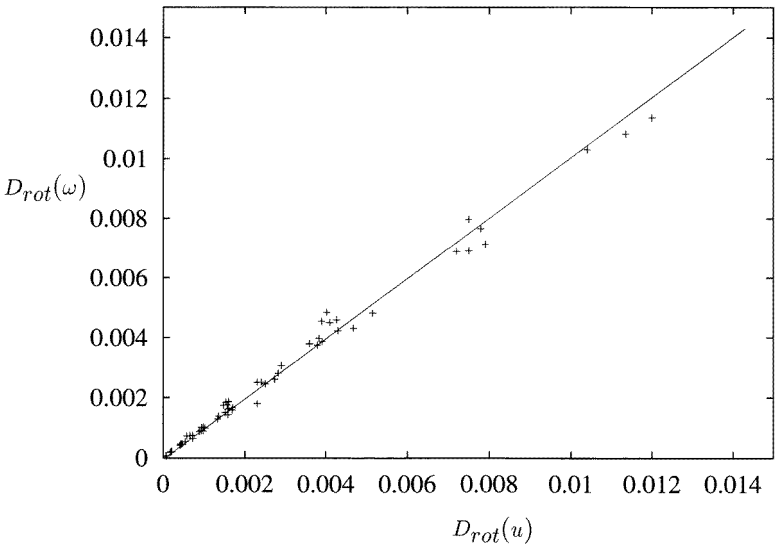


**Figure 10.** A plot of $D_{rot}$ obtained from $C_\omega(t)$ from equation (13), called $D_{rot}(\omega)$, against $D_{rot}$ obtained from $C^1(t)$ and equation (10), called $D_{rot}(u)$.

The rotational diffusion coefficients can be obtained either from $C_\omega(t)$ or $C^1(t)$, which we call $D_{rot}(\omega)$ and $D_{rot}(u)$ respectively. The former method is more convenient for evaluation as it involves an integral of a rapidly decaying function whereas the latter approach (equation (10)) requires a numerical differentiation and some 'judgement' in determining the extent of the inertial regime at short time. Nevertheless, both routes give statistically the same value for the rotational self-diffusion coefficient, as may be seen in figure 10 which plots $D_{rot}(u)$ against $D_{rot}(\omega)$ for all of the systems considered here.

As for the translational degrees of freedom, the mass density of the cluster has a pronounced influence on the short-time rotational dynamics, as may be seen in $C_\omega(t)$. For example, the less massive particles exhibit backscattering in angular velocity but this disappears for more or less equal solvent and nanoparticle mass densities (i.e., $m_c/m = 1$). This is reflected in a $\tau_\omega$ that is extremely sensitive to cluster mass density (see table 1). The less massive clusters have the smallest $\tau_\omega$-values because of the negative backscattering

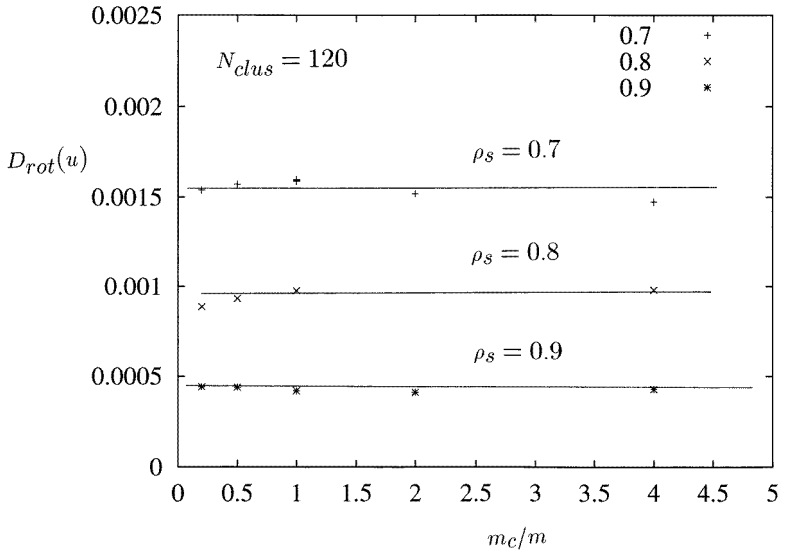


**Figure 11.** The dependence of $D_{rot}$ obtained from $C^1(t)$ on cluster density for $N_{clus} = 120$ particles at three solvent densities.

region at short time leading to a partial cancellation of the positive area under the function. (This effect is compensated for almost exactly in the value of the rotational diffusion coefficient because the moment of inertia is proportional to the cluster mass density i.e., the value of $m_c/m$. We have $D_{rot} = k_B T \tau_\omega / I$.) In contrast, the corresponding $C^1(t)$ are remarkably insensitive to this parameter, which is reflected in a weak dependence of $D_{rot}$ on the mass density of the cluster (as for $D$) but a strong solvent number density and particle size dependence of $D_{rot}$. Figure 11 shows that, as for the translational self-diffusion coefficient, the density of the model nanocolloid in the range covered has little influence, within the simulation statistics, on the value of the rotational diffusion coefficient. In fact, the $\rho_s = 0.7$ results show even less colloid density dependence than the corresponding translational self-diffusion coefficients (compare figures 5 and 11).

The classical solution for rotational diffusion of a macroscopic sphere in a solvent is the Stokes–Einstein–Debye (SED) relationship,

$$D_{rot} = \frac{kT}{8\pi\eta_s a^3} \tag{15}$$

for stick boundary conditions. The cluster radius, $a$, for each cluster was obtained from equation (4). The SED relationship indicates that a plot of $D_{rot}$ against $\sigma_c^{-3}$ should have a slope of $kT/\pi\eta_s$. Figure 12 shows this plot for the $\rho_s = 0.7$ and $\rho_s = 0.9$ fluids. At both solvent densities, the simulation data fall reasonably close to the classical lines, especially for larger clusters.

## 5. Conclusions

In this report we have continued our investigation of the dynamical behaviour of spherical nanocolloids in a solvent represented at the molecular level using the molecular dynamics technique. This work builds upon an earlier study (Heyes *et al* 1996) in which technical

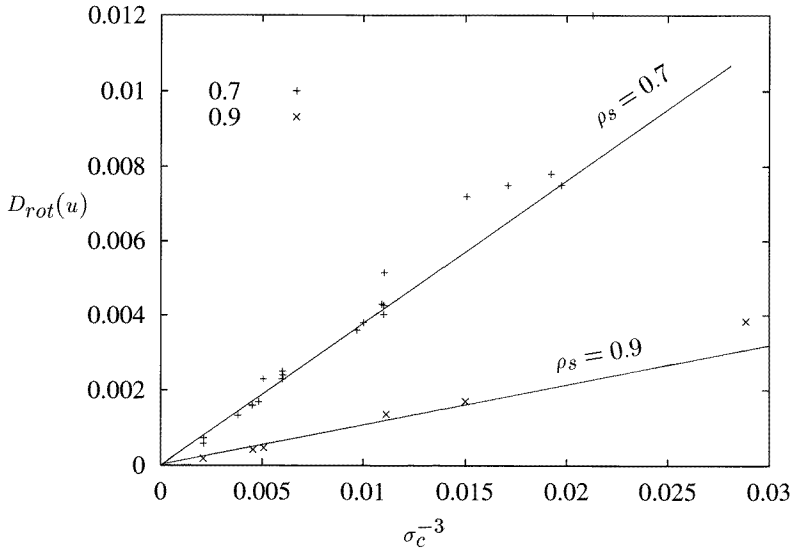


**Figure 12.** A plot of $D_{rot}$ against $\sigma_c^{-3}$. The lines correspond to the SED prediction of equation (15) with a slope of $kT/\pi\eta_s$. Data for the $\rho_s = 0.7$ and $\rho_s = 0.9$ fluids are given, with $\eta_s = 0.84$ and 3.05 respectively (see the legend to figure 6).

aspects of the simulation strategy were developed. The translational and rotational diffusion of the particles have been characterized using time correlation functions, their derived relaxation times and diffusion coefficients. The angular velocity and angular reorientation of the clusters were also computed for the various solvent and nanoparticle specifications.

Simulations were carried out with both smooth and atomistically rough clusters of atoms with variable dimensions compared to the solvent molecule, using the WCA interaction between the colloid and the WCA solvent molecules. Nanocolloidal particles up to an order of magnitude larger than those of the solvent molecule were simulated. The effects of solvent and colloidal particle density, and colloid size on the translational and rotational self-diffusion coefficients were investigated. At liquid-like densities ($\rho_s = 0.9$) the translational, $D$, and rotational, $D_{rot}$, self-diffusion coefficients for the nanocolloids of all sizes were statistically independent of the ratio of colloidal to solvent particle density in the range 0.2–4.0 explored. The rotational diffusion was in accord with the classical 'small-step' limit. As solvent density decreased the translational self-diffusion coefficients of the colloidal particles showed more evidence of a decrease with increasing colloid mass density than did the rotational self-diffusion coefficients. Both $D$ and $D_{rot}$ decreased with increasing size of the colloidal particle and increasing solvent density, largely according to the respective classical solutions given by the Stokes–Einstein and Stokes–Einstein–Debye equations. Differences in the translational diffusion coefficients of smooth and rough colloidal particles were not statistically significant at $\rho_s = 0.9$, but at $\rho_s = 0.7$ were lower for the rough particles, suggesting a larger hydrodynamic radius than the nominal diameter of the colloidal particle, or alternatively some significant solvent restructuring around the colloidal particle at the lower solvent density which was not feasible at higher density owing to excluded-volume constraints within the solvent. Although not carried out here, it would be interesting to investigate the solvent's local structure around the surface of the nanoparticle and also the hydrodynamic radius of the particle by a more direct method.

**Acknowledgments**

This project was partly supported by the Spanish DGICYT (Project No PB95-0254) and by Junta de Extremadura (Consejería de Educación y Juventud). The authors thank the British Council and Delegación de Investigación y Ciencia for supporting this work under the Collaboration Project (Acciones Integradas) between the UK and Spain. The Engineering and Physical Sciences Research Council of Great Britain (EPSRC) is thanked for providing the funding for the DIGITAL AlphaStations workstations used to carry out these simulations.

## References

Bajan-Nunez M C and Dickinson E 1994 *J. Chem. Soc. Faraday Trans.* I **90** 2727
Beck T L, Jellinek J and Berry R S 1987 *J. Chem. Phys.* **87** 545
Benzi R, Succi S and Vergasola M 1992 *Phys. Rep.* **222** 1
Clarke J H R 1978 *Adv. Infrared Raman Spectrosc.* **4** 109
Ermak D L 1975 *J. Chem. Phys.* **62** 4189
Espagñol P and Zúñiga I 1995 *Int. J. Mod. Phys.* **9** 469
Fincham D and Heyes D M 1985 Recent advances in molecular-dynamics computer simulation *Dynamical Processes in Condensed Matter (Advances in Chemical Physics)* ed M Evans (New York: Wiley) pp 493–575
Hansen J-P and McDonald I R 1986 *Theory of Simple Liquids* 2nd edn (London: Academic)
Heyes D M, Nuevo M J and Morales J J 1996 *Mol. Phys.* **88** 1503
Hinch E J 1975 *J. Fluid Mech.* **72** 499
Marsh C A, Backx G and Ernst M H 1997 *Phys. Rev.* E **56** 1676
Nuevo M J, Morales J J and Heyes D M 1995 *Phys. Rev.* E **51** 2026
Rull L F, de Miguel E, Morales J J and Nuevo M J 1989 *Phys. Rev.* A **40** 5856
Spiegel M R 1967 *Theory and Problems of Theoretical Mechanics (Schaum's Outline Series)* (New York: McGraw-Hill) p 226
Stillinger F H and Stillinger D K 1990 *J. Chem. Phys.* **93** 6013
Tildesley D J and Madden P A 1983 *Mol. Phys.* **48** 129
Weeks J D, Chandler D and Anderson H C 1971 *J. Chem. Phys.* **54** 5237
Weitz D A, Pine D J, Pusey P N and Tough R J A 1989 *Phys. Rev. Lett.* **63** 1747
Zhu J X, Durian D J, Müller J, Weitz D A and Pine D J 1992 *Phys. Rev. Lett.* **68** 2559